JOURNAL OF MULTIFUNCTIONAL MATERIALS & PHOTOSCIENCE
5(2), December 2014, pp. 153-170

Review for Semiconductor/reduced Graphene Oxide Nanocomposites: Fabrication, Characterization and Application for Decontamination of Organic Dyes

ZHU Lei, OH Won-Chun

Department of Advanced Materials Science & Engineering, Hanseo University, Seosan-si Chungnam-do, Korea, 356-706

Abstract: Graphene, as an ideal two-dimensional material and single-atom layer of graphite, has attracted exploding interests in multidisciplinary research because of its unique structure and exceptional physicochemical properties. Especially, graphene-based materials offer a wide range of potentialities for environmental remediation and energy applications. This review shows an extensive overview of the main principles and the recent synthetic technologies about designing and fabricating various innovative graphene-based materials. This review highlights the use of graphene nanomaterials in synergy with TiO_2 or other semiconductor examing the approaches and opportunities for enhancement of organic dyes degradation efficiencies. Proposed mechanisms of enhancement, synthesis routes, demonstrations of performance and applications reported in the literature are summarized.

1. Introduction

Graphene is defined as a flat monolayer of carbon atoms tightly packed into a two-dimensional (2D) honeycomb lattice [1]. Graphene is recognized as the basic building block of all-dimensional carbon materials, including 0D fullerene (C60), 1D carbon nanotubes (CNTs), or stacked into 3D graphite, considering wrapped into fullerene, rolled into CNT, or stacked into graphite [2].

Graphene is predicted to have remarkable properties, such as high thermal conductivity, superior mechanical properties, and excellent electronic transport properties [3]. Graphene, with its high specific surface area, excellent transparency, and superior electron mobility, and high chemical stability, graphene can be used as an ideal high performance candidate for catalyst carrier or promoter [4].

Graphene-based composite materials have attracted much attention as recent studies have shown their usefulness in electronics, photocatalysis and photovoltaic devices [5–

*Corresponding author: *wc_oh@hanseo.ac.kr*

7]. Graphene is able to enhance charge transport in a multitude of devices owing to its unique structure: an abundance of delocalized electrons within its conjugated sp2-bonded graphitic carbon network enables graphene with excellent conductivity. To date, various metals–RGO and metal oxide–RGO nanocomposites including palladium, silver, gold, TiO_2, Co_3O_4 and CdSe particles have been reported [8–13]. Typically, these are synthesized using GO as the precursor followed by its reduction to partially restore the conductivity of the pristine graphene. These reduction methods of GO are in large extent dominated by chemical reduction using highly toxic hydrazine and hydrazine derivatives [14,15], thermal reduction [16], electrochemical reduction [17,18], solvothermal reduction [19] and sonolytic reduction [20]. Though effective, some of these methods are not energy and environmentally friendly as toxic substance and high temperature are required.

Recently, Liu *et al.* prepared the self-assembly of TiO_2 with graphene composites in the stabilization of graphene in aqueous solution by assistance of anionic sulfate surfactant [21]. Chen *et al.* prepared a visible-light responsive GO/TiO_2 composite with p/n heterojunction by adding sodium dodecylsulfate in an aqueous of $TiCl_3$ and GO, in which TiO_2 could be excited by visible light with wavelengths longer than 510 nm [22]. Some people synthesized graphene/TiO_2 composites using graphene oxide and P25 as reactants by a facile one-step hydrothermal method and obtained higher photocatalytic activity [23,24]. The principle of this photocatalytic reduction lies on the ability of GO to undergo reduction when it accepts electrons from the excited TiO_2. As photocatalytic reaction does not require stringent experimental conditions such as involving toxic substances and higher temperature, it provides an alternative to prepare graphene-based composite in a greener and safer way. Since TiO2 possesses highly negative conduction band energy, upon excitation with UV illumination, transfer of photogenerated electrons from their conduction bands to GO takes place efficiently. However, the applicability of the photocatalytic reduction of GO has not yet been proven in a wider context of photocatalysis as many visible light active photocatalysts are known for their much lower conduction band energy than the UV active TiO_2.

In addition, the high recombining probability of electrons and holes photogenerated in TiO_2 would decrease its photocatalytic activity. All these drawbacks limit its application especially in the large-scale industry. To solve the above problems, many methods have been applied to extend the light absorption of TiO_2 into the visible region and increase its photocatalytic activity. Compared with other materials, semiconductors (or quantum dots) have attracted considerable interest in the past two decades because of their applications in single electron transistors, lasers, light emitting diodes, and infrared photodetectors operating at lower currents and higher temperatures. Various semiconductors, including CdS [25], PbS [26], Bi_2Se_3 [27], ZnSe [28], have been investigated to sensitize TiO_2 as a visible light absorber.

In this work, we present our studies on the utilization of a range of photocatalysts including UV driven TiO_2 and visible light active Bi_2Se_3, ZnSe to study the effectiveness of GO photocatalytic reduction.

2. Synthesis of Graphene Oxide (GO) [29]

Graphite (KS-6) was selected as the starting material. Graphene oxide (GO) was prepared from graphite according to the Hummers-Oûeman method [30]. In brief, graphite powder (10 g) was dispersed in cold concentrated sulphuric acid (230 mL, 98 wt%, dry ice bath), and potassium permanganate ($KMnO_4$, 30 g) were gradually added with continuous vigorous stirring and cooling to prevent the temperature from exceeding 293 K. The dry ice bath was removed and replaced by a water bath, and the mixture were heated to 308 K for 30 min with gas release under continuous stirring, followed by slow addition of deionized water (460 mL), which produced a rapid increase in solution temperature up to a maximum of 371 K. The reaction was maintained for 40 min in order to increase the oxidation degree of the GO product; then the resultant bright-yellow suspension was terminated by addition of more distilled water (230mL), followed by a hydrogen peroxide solution (H_2O_2, 30%, 250 mL). The solid products was separated by centrifugation at 3000 rpm, was washed initially with 5% HCl until sulphate ions were no longer detectable with barium chloride ($BaCl_2$), were then washed three times with acetone, and were air dried overnight in vaccum oven. After sonication for 30 min under 308K, the graphite oxide was transformed into graphene oxide sheet [31]. The preparation procedure is shown in Fig. 1.

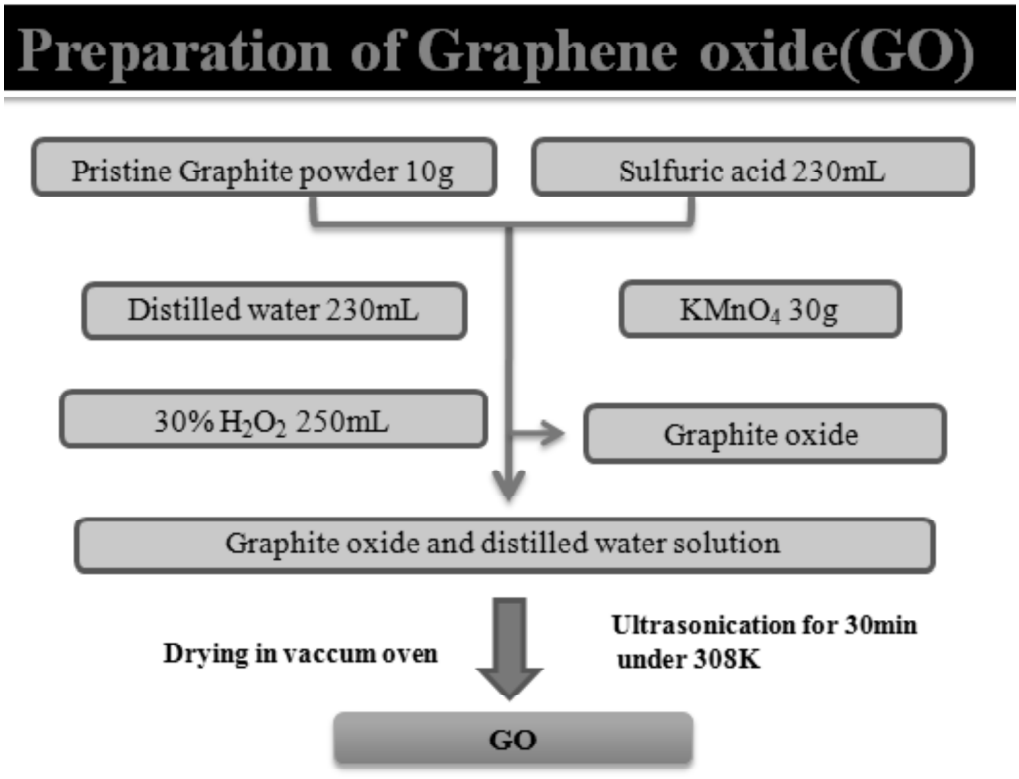

Figure 1: Schematic Diagram Showing the Procedure for Synthesis of GO [29]

3. TiO_2-Graphene Nanocomposite for the Enhancement Photocatalytic Effect

The direct growth of the TiO_2 precursors on GO sheets and absorbed on them were achieved by a sonochemical method. And a proposed mechanism of ultrasonic-assisted synthesis was described in Fig. 2.

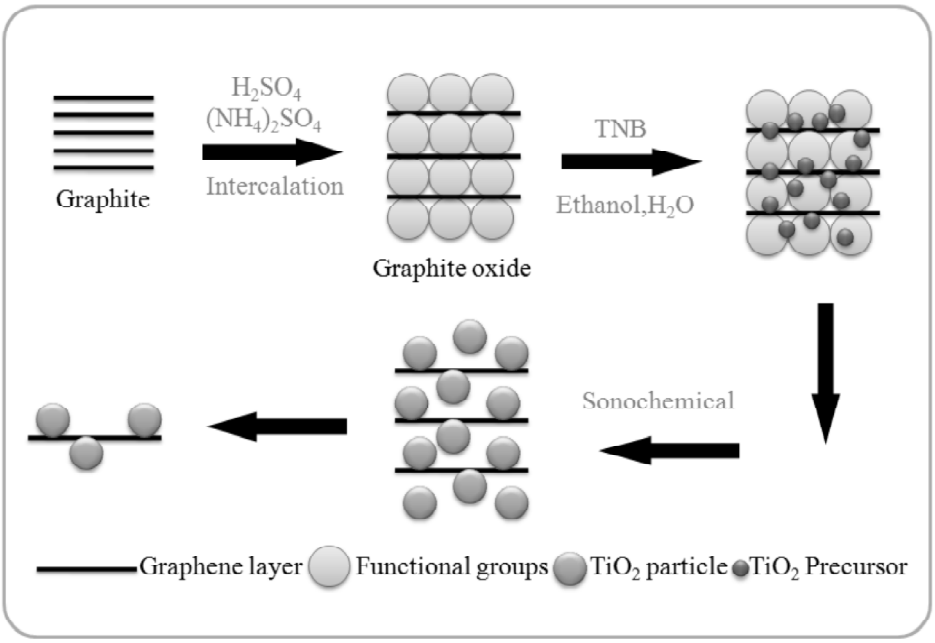

Figure 2: The Proposed TiO_2 Nanoparticles Formation Mechanism on the Graphene Sheets by Sonochemical Method [29]

We used raman spectroscopy to examine the changes that occurred in the crystal structure of the GR–TiO_2-2 and GO, as shown in Fig. 3. The Raman spectra of GO (inset graph in Fig. 3) show the presence of D and G bands at 1345 and 1592 cm^{-1}, respectively. G band is common to all sp^2 carbon forms and provides information on the in-plane vibration of sp^2 bonded carbon atoms. The D band suggests the presence of sp^3 defects. The second-order Raman feature, namely the 2D band (second-order of the D band) at about 2720 cm^{-1}, is very sensitive to the stacking order of the graphene sheets along the c-axis as well as to the number of layers, and shows greater structure (often a doublet) with increasing number of graphene layers. The stacking structure and agglomerated morphology of the GO nanosheets are therefore consistent with previous report. In the raman spectrum of GR–TiO_2-2, the G band is broadened and shifted to 1354 cm^{-1} in Fig. 3. In addition, D band shifted to around 1602 cm^{-1}, respectively. Simultaneously, relative intensity of D/G was increased after hydrothermal reaction, which is in agreement with reported by Lambert [32] and Stankovich [14] *et al.* This further confirmed that GO was reduced to graphene and indicate the considerable increase in size of the in-plane sp^2 domains and thickness of graphitic structure due to hydrothermal reaction.

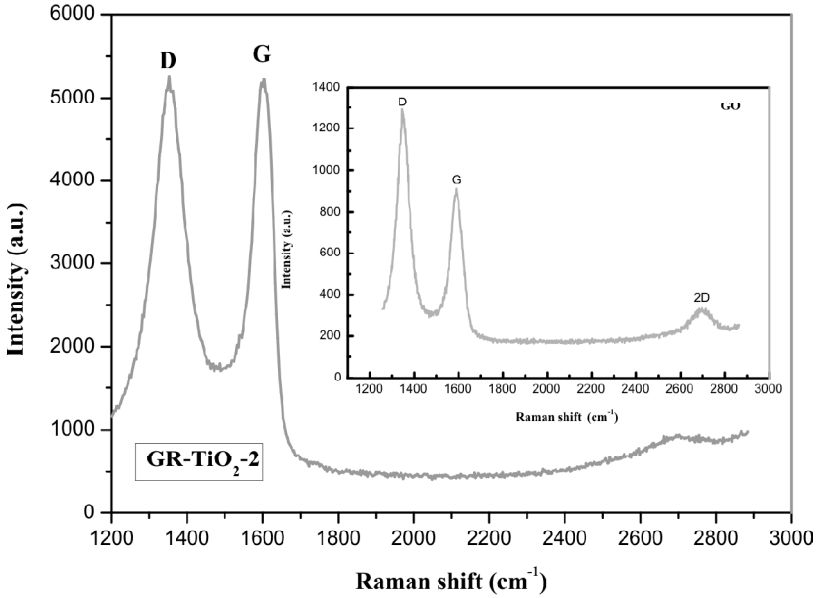

Figure 3: Raman Spectra of GR–TiO_2-2 Nanocomposite and GO [29]

Fig. 4. shows the XRD peak patterns of graphene and GR-TiO_2 composites. Typical (002) and (100) peaks of graphene (Fig. 6 (a)) were observed at 2θ of ~26° and ~43°, respectively, which could be indexed to the characteristic peaks (002) and (100) plane reflections of graphite from the graphene (JCPDS No. 01-0646). Moreover, no typical diffraction peaks belonged to graphene can be found in these curves, indicates that the GO has been reduced to graphene during the hydrothermal reaction, which is in agreement with early reports. In comparison of the patterns of nanoscale TiO_2, the XRD diffraction peaks around 2θ of 37.9°, 47.8°, 54.3°, 55° and 62.7°, which could be indexed to the characteristic peaks (004), (200), (105), (211) and (204) of anatase TiO_2 (JCPDS No. 21-1272), can be observed in all of GR-TiO_2 composites. There no peaks around of 27.4°, 36.1°, 41.2° and 54.3° belong to the diffraction peaks of (110), (101), (111) and (211) of rutile (JCPDS No. 21-1276). It can be indicated that the anatase form is dominant in all of the as-prepared composites prepared through the sonochemical reaction process.

The typical micro-surface structures and morphologies of as-obtained TiO_2 and GR-TiO_2 composite was displayed in Fig. 5 (a-d). Nanoscale TiO_2 displayed well-dispersed nanoparticles with an average size of around 10 to 15 nm, can be clearly seen in Fig. 5 (a). Fig. 5 (b-d) reveals a homogeneous dispersion of TiO_2 nanoparticles attached onto the almost transparent graphene sheets, which may play a support material role in helping TiO_2 crystals growth. In this reaction approach, the reduction of GO and the deposition of TiO_2 nanoparticle on graphene occur simultaneously. Once the reaction was complete, TiO_2-decoration helps to prevent not only the aggregation of the graphene sheets, but also the aggregation of TiO_2. The formation mechanism of TiO_2 particle itself and the exact role of graphene sheets in this process still await further studies.

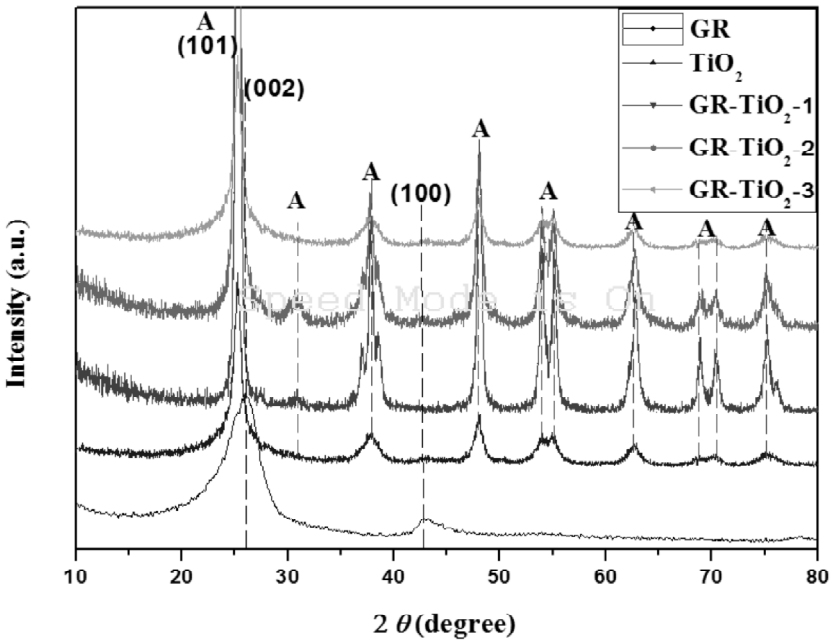

Figure 4: XRD Analysis of GR, TiO_2 and GR-TiO_2 Photocatalyst [29]

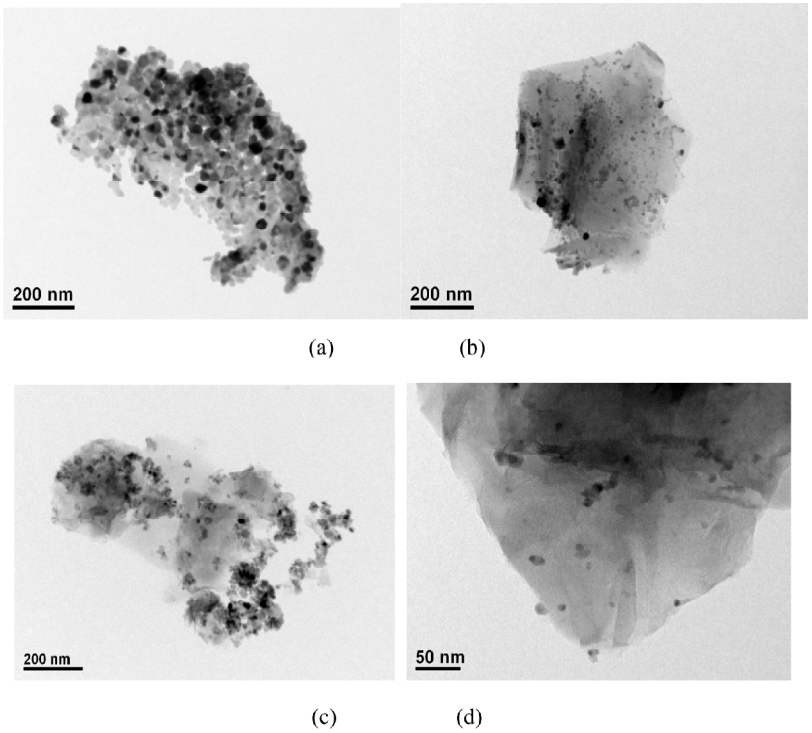

Figure 5: SEM and TEM micrographs of as-prepared samples: (a, d) GR, (a) nanoscale TiO_2, (b) GR-TiO_2-1, (c) GR-TiO_2-2, (d) GR-TiO_2-3 [29]

The effect of ultrasonic irradiation on RhB degradation by the nanoscale TiO_2 and GR–TiO_2 composite catalyst were investigated tentatively, in Fig. 10. We compare the decontamination effect between ultrasonic, control sample, nanoscale TiO_2 and GR–TiO_2. From Fig. 6 (a), we can ûnd that after ultrasonic irradiation 150 min, the degradation effect of GR–TiO_2–2 is the best (88.66%), while the degradation ratio of GR–TiO_2–1and GR–TiO_2–2 for Rh. B solution is 33.31% and 58.71%, and 4.8% with only ultrasonic irradiate, respectively. All calculated -ln(C/C_t) values were approximately linear with the irradiation time listed in Fig.6 (b). Therefore, the sonocatalytic degradation process of Rh.B on these six sonocatalytic points obeys ûrst-order kinetics. Irradiation with the ultrasound for 150 min caused a signiûcant decrease, which indicates that the degradation rate was quite rapid. On the other hand, the degradation rate in the presence of bare TiO_2 was lower than that of the GR–TiO_2 composite catalyst.

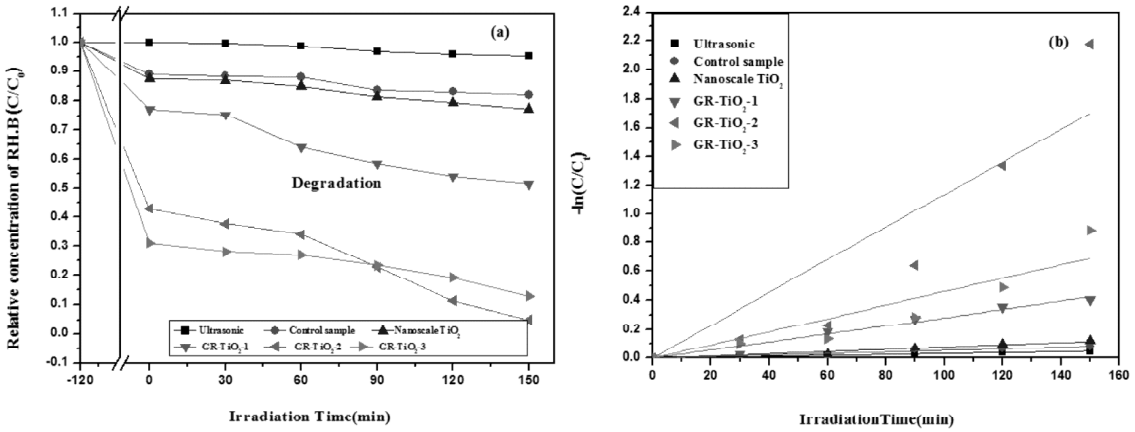

Figure 6: Decolorization Effect (a) and Apparent First order Kinetics (b) of Rh.B for Sonocatalyst [29]

4. Bi_2Se_3-Graphene/TiO2 Nanocomposites for the Enhancement Sonophotocatalytic Effect

Bi_2Se_3 has a band gap (0.3eV) samller than TiO_2 (3.2 eV), this makes it possible to use Bi_2Se_3 as a photosensitizer for TiO_2 by injecting the conduction band electron from Bi_2Se_3 to TiO_2[27]. Herein we obtained chemically bonded Bi_2S_3-Graphene/TiO_2 composites using a facile microwave-assisted synthesis method, and a proposed mechanism was described in Fig. 7. During the hydrothermal reaction, both of the reduction of graphene oxide to graphene and loading of Bi_2Se_3 and TiO_2 particles on graphene nanosheet were achieved.

Fig. 8 shows the X-ray diffraction patterns of the as-prepared pure TiO_2, Bi_2Se_3, GR - TiO_2 and Bi_2Se_3-GR/TiO_2 composites sonophotocatalysts. According to the results, (101), (004), (200), (105), (211), and (204) crystal planes are originated from the anatase TiO_2 phase (JCPDS file, No. 21-1272), while all of the reflection peaks of the XRD pattern can be indexed to rhombohedral (hexagonal) Bi_2Se_3, with calculated lattice parameters of a = 4.1716Å and c = 27.696Å. These values correspond to published lattice parameters of a = 4.1396Å and c = 28.636Å (JCPD33-214) [34]. No reflection peaks of impurities are

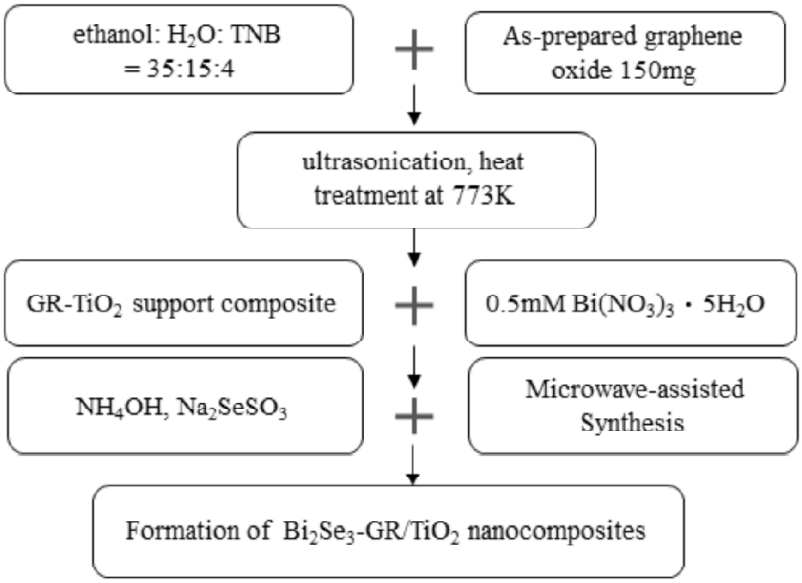

Figure 7: Flow Chart to Prepare Bi_2Se_3-GR/TiO_2 Nanocomposites[33]

observed, indicating the high purity of the products. However, no signal for any other phases about GO (001) or graphene (002) can be detected in GR-TiO_2 and Bi_2S_3-GR/TiO_2 composite. GO can be reduced to graphene during the reaction and the synthesized graphene sheets can restack to form poorly ordered graphite along the stacking direction. Earlier studies have shown that if the regular stack of GO or graphite is broken, for example, by exfoliation, their diffraction peaks may also become weak or even disappear.

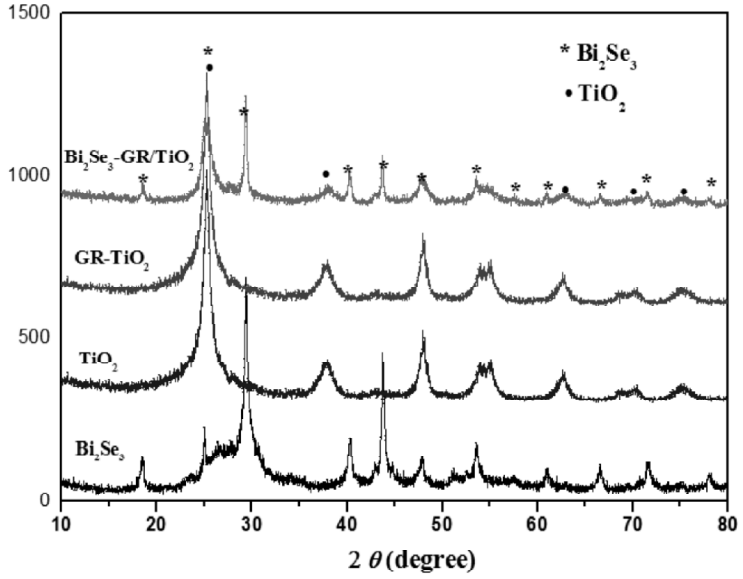

Figure 8: XRD Analysis of Pure Bi_2Se_3, TiO_2, GR-TiO_2 and Bi_2Se_3-GR/TiO_2 Composite[33]

In order to check the visible photo-response of the pure TiO_2, GR-TiO_2 and Bi_2Se_3-GR/TiO_2 composites, UV-vis absorption spectras were presented in Fig. 9. As expected, the spectrum obtained from the pure TiO_2 and GR-TiO_2 composites shows that TiO_2 absorbs mainly the ultraviolet light with absorption wavelength below 400 nm. Compared with pure TiO_2, a shift of the intense absorbance edge of GR-TiO_2 and Bi_2Se_3-GR/TiO_2 composites towards the visible light region was observed and the absorption edge at approximately 738 nm. The absorbance spectra of Bi_2Se_3-GR/TiO_2 composite as-formed show an intense absorption and have a red-shift absorption onset comparing with both TiO_2 and GR-TiO_2.

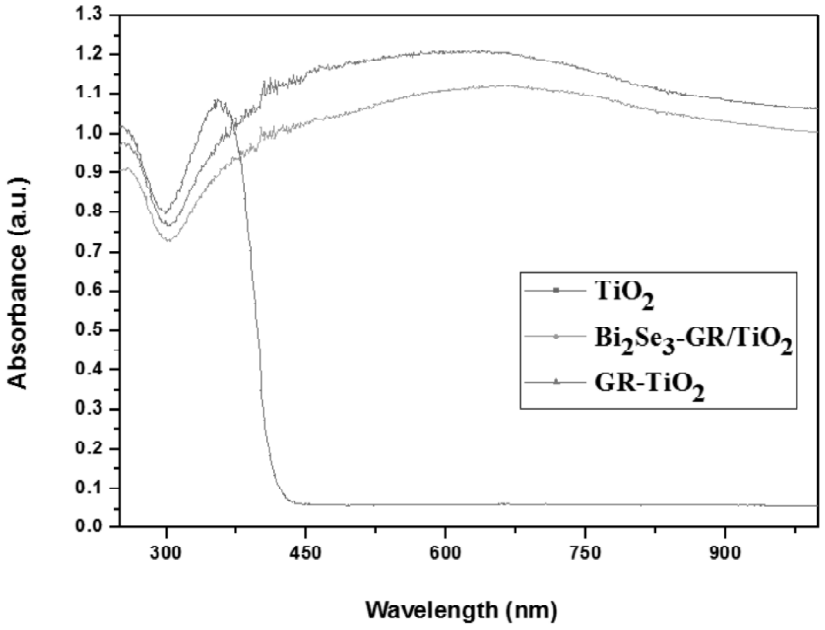

Figure 9: UV-vis Adsorption Spectra of Pure TiO_2, GR-TiO_2 and Bi_2Se_3-GR/TiO_2 Composite [33]

Fig. 10a shows the photocatalytic activity of pure TiO_2, Bi_2Se_3-TiO_2, GR-TiO_2 and Bi_2Se_3-GR/TiO_2 composite photocatalysts evaluated by the decomposition of Rh.B solution under visible light irradiation for 120min. As shown in Fig. 10b, the absorbance values for Bi_2Se_3-GR/TiO_2 composite decreased with an increase of visible light irradiation time. The Bi_2Se_3/TiO_2 composite showed the remarkable and fast adsorption capacity of Rh.B solution than pristine TiO_2. The adsorption effect of GR-TiO_2 is better than that of any other samples due to the relatively higher surface area. The photocatalytic degradation of Rh.B solution with Bi_2Se_3-GR/TiO_2 composite was better than any other composites, Rh.B solution with high concentration is removed 45.4% after visible light irradiation for 120min. As mentioned above in surface characteristics, the favorable morphology could play an important role in shuttling visible light photo-induced electrons generated from Bi_2Se_3 into the conduction band of TiO_2 efficiently.

It suggested that the combination of photocatalysis and sonolysis is more effective in dye degradation. Ultrasound may promote the rate of photocatalytic degradation by

modifying the deaggregation of the catalyst to increase its active surface area. Thus, in order to obtain the sonophotocatalytic activity for Bi_2Se_3-GR/TiO_2 composite, the concentration was increased to 2×10^{-5} M. The sonophotocatalysis results were shown in Fig. 11. The results clearly show that the Rh.B degradation efficiency of visible light

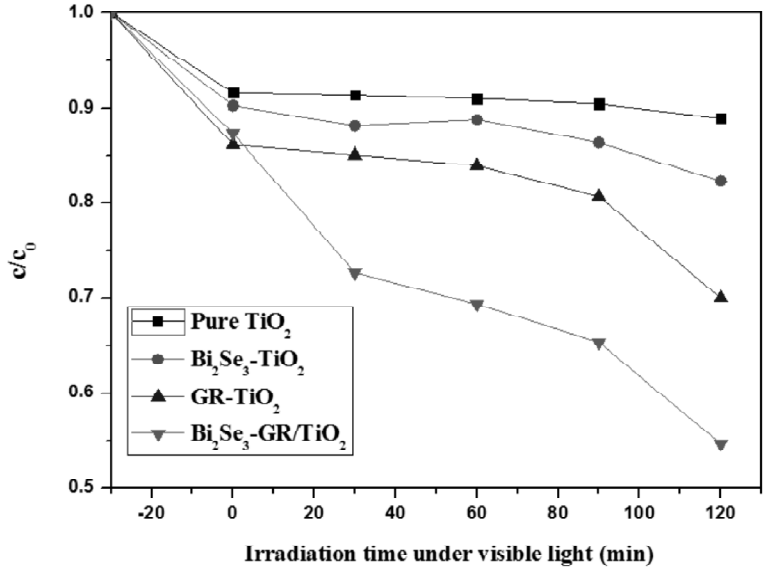

(a)

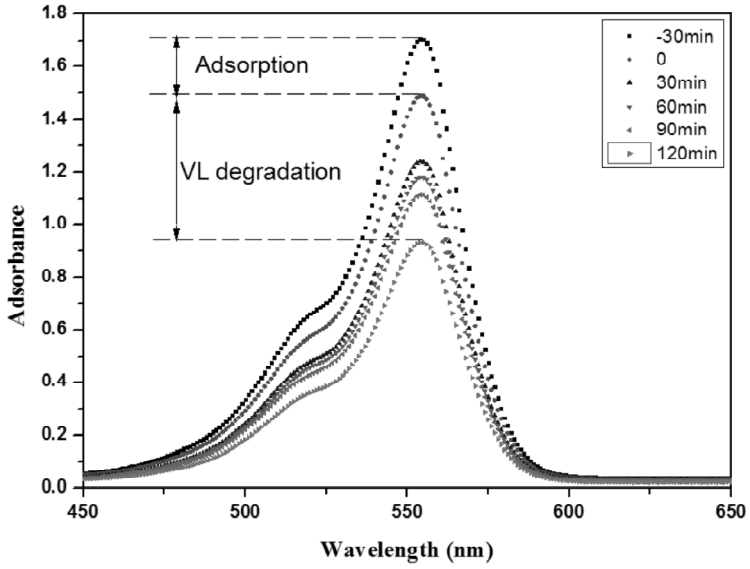

(b)

Figure 10: (a) Degradation of Rh.B dye (3×10^{-5} mol/L, 50 mL) with different samples (0.03 g); (b) UV/Vis spectra of Rh.B concentration against the Bi_2Se_3-GR/TiO_2 composite under visible light for 120 min[33]

photocatalysis for 120 min was 37% while sonophotocatalysis for the same time was 59%. This is due to photocatalyst can be excited by ultrasound-induced luminescence which has a wide wavelength and increased production of hydroxyl radicals (.OH) in the reaction mixture. It can be also indicated that the prepared Bi_2Se_3-GR/TiO_2 composite shows high degradation activity not only under visible light but also under ultrasonic.

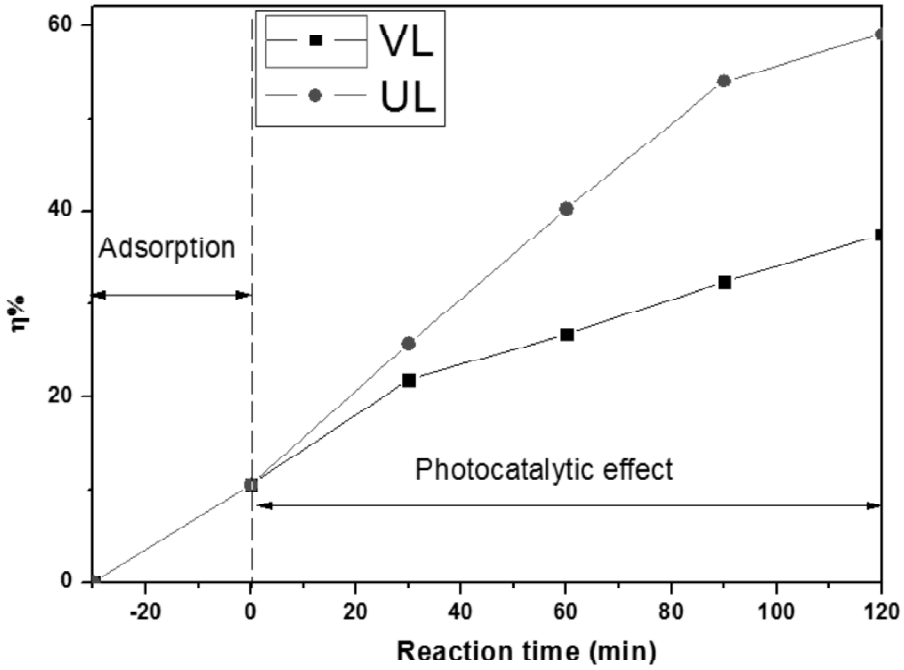

Figure 11: Degradation efficiency of Rh.B solution by Bi_2Se_3-GR/TiO_2 composite under irradiation of visible light (VL) and ultrasonic combined visible light(UL). The concentration of organic dyes is 2×10^{-5} M; the amount of Bi_2Se_3-GR/TiO_2 composite is 0.03 g[33]

5. ZnSe-Graphene/TiO_2 Nanocomposites for the Enhancement Photocatalytic Effect

Another important feature of the coupled semiconductor system is that the photoresponse of a large band gap semiconductor can be extended into the visible region by coupling it with a short band gap semiconductor. Metal selenides have attracted much attention during the past fewyears due to their special electronic and optical properties and potential applications ZnSe is a wide direct band gap compound semiconductor which has received much attention for their potential applications in optoelectronics and electronics [36]. ZnSe is particularly suitable for applications for blue-green laser diodes and tunable mid-IR laser sources for remote sensing. ZnSe has a direct band gap of ~ 2.7 eV with a conduction band of ~ 0 eV and a valence band of ~ 2.7 eV, making it well suited for solar applications. The low bandgap of ZnSe makes it can absorb light in wider spectrum range. In theory, TiO_2 with a conduction band of ~ -0.2 eV and a valence band of ~ 3.0 eV ; so when ZnSe are attached to the surface of the TiO_2, the relative position of the ZnSe CB edge permits the transfer of electrons from the TiO_2 surface to ZnSe. Simultaneously, ZnSe can absorb

photons and excite photoelectron from VB to CB. The transfer of the electrons between TiO_2 and ZnSe leads to enhanced photocatalysis performances of the composite ZnSe/TiO_2.

XRD analysis was used to determine the phase purity and the average crystalline properties of ZnSe-GR/TiO_2 composites shown in Fig. 12. Comparison with the patterns of pure TiO_2, the XRD diffraction peaks around 2θ of 37.9°, 47.8°, 54.3°, 55° and 62.7°, which could be indexed to the characteristic peaks (004), (200), (105), (101), (211) and (204) of anatase TiO_2 (JCPDS No. 21-1272), while (111), (220), (311) of ZnSe crystal planes was originated from the zinc blende structure (JCPDS Card No. 21-1272), which were in accordance with the results reported by ThanhThuy et.al with the lattice parameters [28]. Weak new peaks are appeared at different degree about 30° and 34°, when the reaction condition is 160 °C, 6h. It may be due to the presence of ZnO phase in the composite, when the reaction is not so long which was in accordance with the research by Soodabe Gharibe. However, no signal for any other phases about GO (001) or graphene (002) can be detected in GR-TiO_2 and ZnSe-GR/TiO_2 composite. GO can be reduced to graphene during the solvothermal reaction and the synthesized graphene sheets can restack to form poorly ordered graphite along the stacking direction. Earlier studies have shown that if the regular stack of GO or graphite is broken, for example, by exfoliation, their diffraction peaks may also become weak or even disappear.

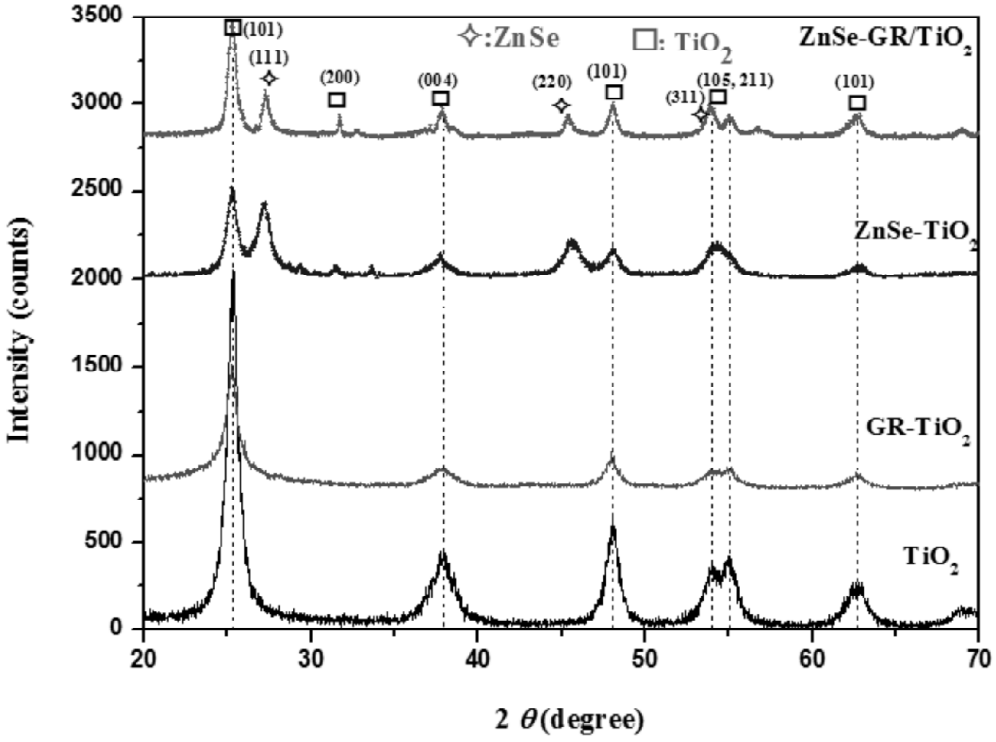

Figure 12: XRD Patterns of as-prepared Samples: (a) pure TiO_2, (b) GR-TiO_2, (c) ZnSe-TiO_2, (d) ZnSe-GR/TiO_2 [35]

TEM images of ZnSe/TiO_2 and ZnSe-GR/TiO_2 nanocomposites with different magnification are well observed in Fig. 13. The composite exhibit uniform size distribution and the TiO_2 particles are cubic-shaped with the average size of 15 to 20 nm, the average size of well-dispersed ZnSe nanoparticles was around 10 to 15 nm. And the lattice spacing of 0.35nm was assigned to the (101) plane of highly crystalline anatase phase, being in good agreement with early report. And the interplanar spacings of (110) lattice plane families of ZnSe with a lattice parameter of α = 0.567nm. The presence of the GR as a template leads to a lower aggregation of the TiO_2 and ZnSe nanoparticles. In return, the TiO_2 and ZnSe nanoparticles can also prevent the agglomeration of GR sheets after reduction process.

An interesting alternative to the degradation of pollutants in waste water is sonocatalysis, which can be used instead of photocatalysis. The effect of ultrasonic

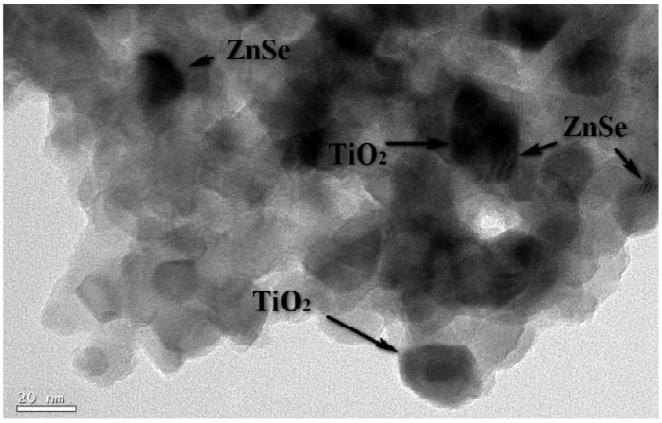

(a)

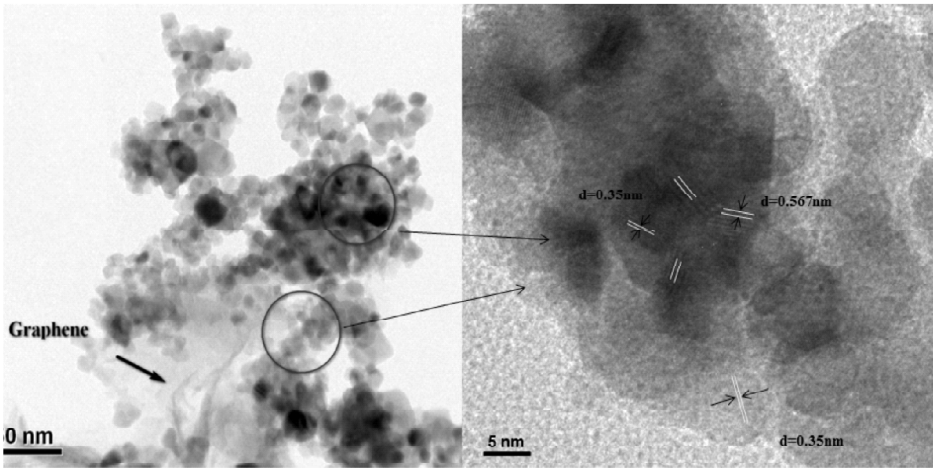

(b)

Figure 13: TEM Micrographs of as-prepared Samples: (a) ZnSe/TiO_2, (b) ZnSe-GR/TiO_2 [35]

irradiation on RhB degradation by the pure TiO_2, GR-TiO_2, ZnSe/TiO_2 and ZnSe-GR/TiO_2 composite catalysts were investigated tentatively, in Fig. 14. From Fig. 14 a, we can ûnd that after ultrasonic irradiation 150 min, the degradation effect of ZnSe-GR/TiO_2 is the best (82.9%), while the degradation ratio of GR–TiO_2 and ZnSe/TiO_2 for Rh. B solution is 47.3% and 34.1%. All calculated -ln(C_t/C_{ads}) values (with the restriction of C_{ads} being the

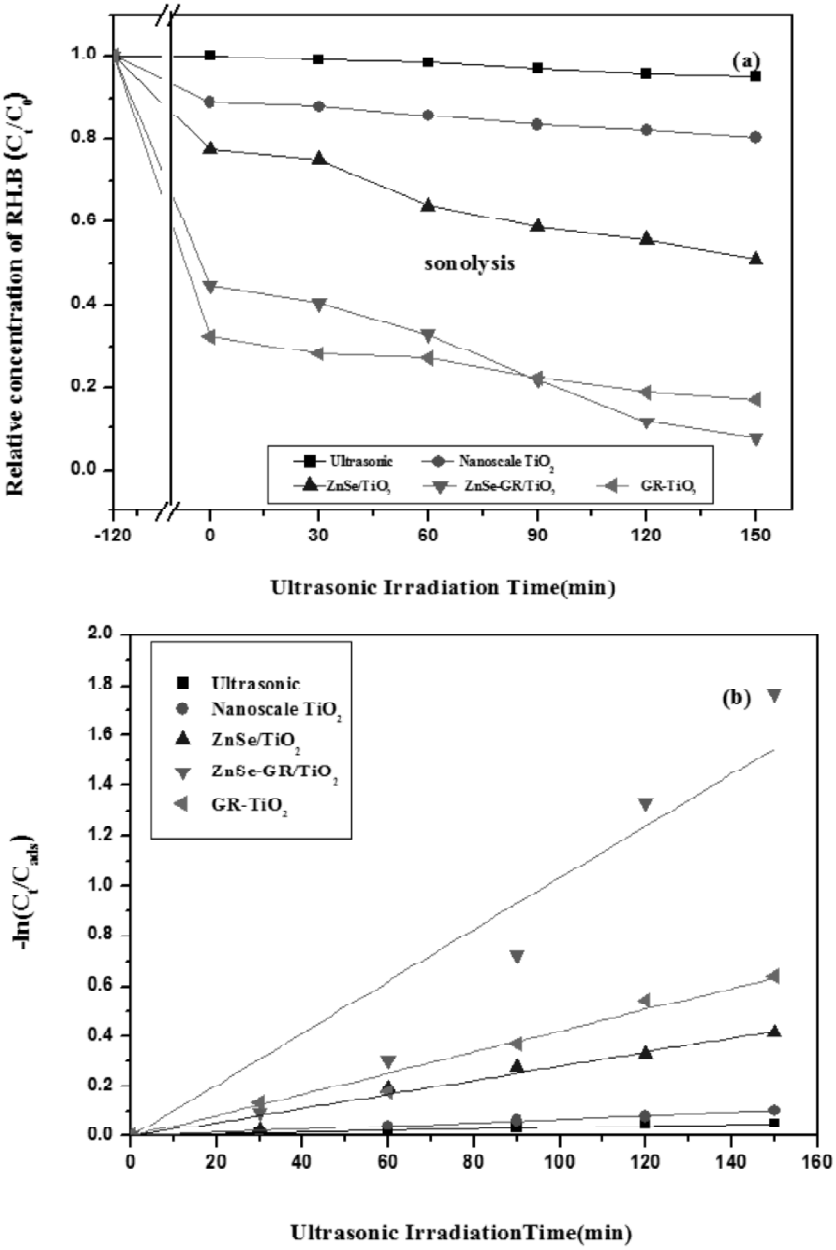

Figure 14: Decolorization effect (a) and apparent first order kinetics (b) of Rh.B degradation over pure TiO_2, ZnSe/TiO_2, GR-TiO_2 and ZnSe-GR/TiO_2 under ultrasonic irradiation [35]

initial concentration in the bulk solution after dark adsorption and t being the sonolysis reaction time) were approximately linear with the irradiation time represented in Fig. 14 b. The Rh.B degradation rate constant for ZnSe-GR/TiO_2 composites reaches 10.32×10^{-3} min^{-1} under ultrasonic irradiation, which was much higher than the corresponding values for pure TiO_2, GR-TiO_2 and ZnSe/TiO_2.

Sonocatalytic degradation of the dyes in presence of bare TiO_2 has been reported in several papers. The oxidation process of dyes is $OH^{\bullet}$ dependent, which can be explained by the well-known mechanism of hot spots and sonoluminescence as follows. First, cavitation can be increased by the heterogeneous nucleation of bubbles, resulting in the induction of hot spots in solution. These hot spots can cause the pyrolysis of H_2O molecules to form $^{\bullet}OH$ pressure (Eq. (1)). Second, sonoluminescence involves an intense UV-light, which excite the TiO_2 particles to act as a photocatalyst during sonication. Usually sonochemical reaction pathways for the degradation of organic compounds by the sonolysis of water as the solvent inside the collapsing cavitation bubbles under extremely high temperature. In addition, graphene nanosheet acting as good electron acceptors [32] can accept the electrons by light irradiation and the electrons exited in CB of ZnSe are also transferred to the surface of graphene. When added sonocatalytic, the ultrasonic dynamics system not only sonolysis of water but also coupled with induced by the catalyst to produce electron–hole pairs (Eq. (2)). The electron–hole pairs can produce $^{\bullet}OH$ radical and superoxide anion $^{\bullet}O_2^-$, which can decompose the dyes to CO_2, H_2O and inorganic (Eqs. (3)–(5)). These $\bullet OH$ can oxidize 1,5-diphenyl carbazide (DPCI) into 1,5-diphenyl carbazone (DPCO).

$$H_2O+\text{Ultrasonic} \rightarrow {}^{\bullet}OH+{}^{\bullet}H \quad (1)$$

$$ZnSe/TiO_2 + \text{Ultrasonic} \rightarrow ZnSe\ (h+)/TiO_2\ (e-) \quad (2)$$

$$e^- + O_2 \rightarrow {}^{\bullet}O_2^- \quad (3)$$

$$h^+ + H_2O \rightarrow {}^{\bullet}OH \quad (4)$$

$$\text{Sonocatalyst} + \text{Ultrasonic} + H_2O + O_2 + \text{Rh.B} \rightarrow CO_2 + H_2O + \text{inorganic} \quad (5)$$

We propose a mechanism for the degradation of pollutants ZnSe-GR/TiO_2 sonocatalyst under ultrasonic irradiation as shown in Fig. 15.

5. Conclusions

In summary, as a new and unique 2D carbon nanomaterial, graphene has been applied to construct different and promising sorbents and catalysts. The modification of graphene is not only enhancing its specificity, loading capacity, and biocompatibility, but also overcoming some intrinsic drawbacks in the application of environmental preserve and energy-related system. Most importantly, incorporating with nanoparticles or other substances, graphene can offer their unique properties and possibly induce new performance, such as high adsorption capacity, extended light adsorption range, and excellent charge separation–transportation capability. TEM image shows that the surface of graphene has been coated with nanoscale particles. The diffuse reflectance spectra

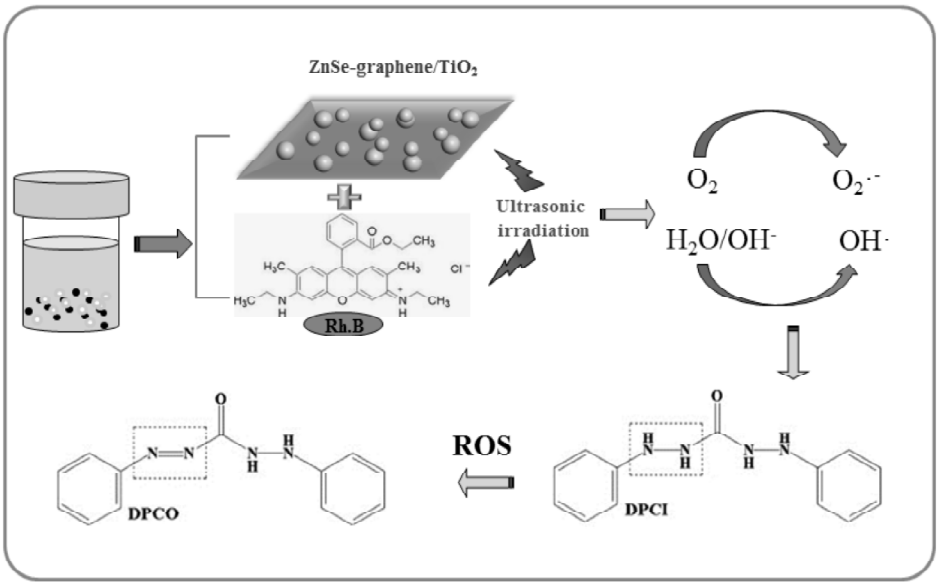

Figure 15: Schematic Drawing of Sonocatalytic Degradation Rh.B and ROS Generation on the Interface of ZnSe-GR/TiO_2 Composite under Ultrasonic Irradiation [35]

suggest the graphene semiconductor composite shows strong photo-absorption at UV light and visible light range. The organic dyes degradation efficiencies of the graphene based semiconductor composite photocatalysts was investigated by degradation of Rh.B or MB organic dyes in aqueous solution under ultrasonic or visible light irradiation. According to the excellent dye degradation results, the decrease in the Rh.B concentration can be ascribed to the two kinds of effects between visible light photocatalysis and sonophotocatalysis. Thus, the expanding of graphene-based materials in the field of adsorption and catalysis science promotes the superior improvement of pollution control and energy development.

Reference

[1] K.S. Novoselov, A.K. Geim, S.V. Morozov, D. Jiang, Y. Zhang, S.V. Dubonos, I.V.Grigorieva, A.A. Firsov, Electric Field Effect in Atomically Thin Carbon Films, Science. 306, (2004), 666.

[2] A.K. Geim, K.S. Novoselov, The rise of graphene, *Nat. Matter.* 6, (2007), 183.

[3] G. Wang, X.Shen, B. Wang, J.Yao, and J. Park, Synthesis and characterization of hydrophilic and organophilic graphene nanosheets, *Carbon*, 47, (2009), 1359.

[4] Y. Sun, Q. Wu, G. Shi, Graphene based new energy materials, *Energy. Environ. Sci.* 4, (2011), 1113.

[5] P.V. Kamat, Anchoring Semiconductor and Metal Nanoparticles on a 2-Dimensional Carbon Support, J. *Phys. Chem. Lett.* 1, (2010), 520.

[6] H. Zhang, X. Lv, Y. Li, Y. Wang, J. Li, P25-Graphene Composite as a High Performance Photocatalyst, *ACS Nano* 4, (2010), 380.

[7] S.R. Kim, M.K. Parvez, M. Chhowalla, UV-reduction of graphene oxide and its application as an interfacial layer to reduce the back-transport reactions in dye-sensitized solar cells, *Chem. Phys. Lett.* 483, (2009), 124.

[8] G.M. Scheuermann, L. Rumi, P. Steurer, W. Bannwarth, R. Mulhaupt, Palladium nanoparticles on graphite oxide and its functionalized graphene derivatives as highly active catalysts for the Suzuki-Miyaura coupling reaction, *J. Am. Chem. Soc.* 131, (2009), 8262.

[9] R. Pasricha, S. Gupta, A.K. Srivastava, A Facile and Novel Synthesis of Ag–Graphene-Based Nanocomposites, Small. 5, (2009), 2253.

[10] R. Muszynski, B. Seger, P.V. Kamat, *J. Phys. Chem*. C 112, (2008,) 5263.

[11] T.N. Lambert, C.A. Chavez, B. Hernandez-Sanchez, P. Lu, N.S. Bell, A. Ambrosini,T. Friedman, T.J. Boyle, D.R. Wheeler, D.L. Huber, Decorating graphene sheets with gold nanoparticles, *J. Phys. Chem. C* 113, (2009), 19812.

[12] Z.S. Wu, W. Ren, L. Wen, L. Gao, J. Zhao, Z. Chen, G. Zhou, F. Li, H.-M. Cheng, Graphene anchored with $Co_{(3)}O_{(4)}$ nanoparticles as anode of lithium ion batteries with enhanced reversible capacity and cyclic performance, ACS Nano. 4, (2010), 3187.

[13] Y. Lin, K. Zhang, W. Chen, Y. Liu, Z. Geng, J. Zeng, N. Pan, L. Yan, X. Wang, J.G. Hou, Dramatically enhanced photoresponse of reduced graphene oxide with linker-free anchored CdSe nanoparticles, ACS Nano. 4, (2010), 3033.

[14] S. Stankovich, D.A. Dikin, R.D. Piner, K.A. Kohlhaas, A. Kleinhammes, Y. Jia, Y. Wu, S.T. Nguyen, R.S. Ruoff, Synthesis of graphene - based nano sheets via chemical reduction of exfoliated graphite oxide, *Carbon*. 45, (2007), 1558.

[15] S. Stankovich, D.A. Dikin, G.H.B. Dommett, K.A. Kohlhaas, E.J. Zimney, E.A. Stach, R.D. Piner, S.T. Nguyen, R.S. Ruoff, Graphene-based composite materials, *Nature*. 442, (2006), 282.

[16] H.C. Schniepp, J.-L. Li, M.J. McAllister, H. Sai, M. Herrera-Alonso, D.H. Adamson, R.K. Prud'homme, R. Car, D.A. Saville, I.A. Aksay, Functionalized single graphene sheets derived from splitting graphite oxide, *J. Phys. Chem. B* 110, (2006), 8535.

[17] H.L. Guo, X.F. Wang, Q.Y. Qian, F.B. Wang, X.H. Xia, A green approach to the synthesis of graphene nanosheets, ACS Nano. 3, (2010), 2653.

[18] S.J. An, Y. Zhu, S.H. Lee, M.D. Stoller, T. Emilsson, S. Park, A. Velamakanni, J. An, R.S. Ruoff, Thin film fabrication and simultaneous anodic reduction of deposited graphene oxide platelets by electrophoretic deposition, *J. Phys. Chem. Lett.* 1, (2010), 1259.

[19] H. Wang, J.T. Robinson, X. Li, H. Dai, Solvothermal reduction of chemically exfoliated graphene sheets, *J. Am. Chem. Soc.* 131, (2009), 9910.

[20] K. Vinodgopal, B. Neppolian, I.V. Lightcap, F. Grieser, M. Ashokkumar, P.V. Kamat, Sonolytic Design of Graphene"Au Nanocomposites. Simultaneous and Sequential Reduction of Graphene Oxide and Au(III), *J. Phys. Chem. Lett.* 1, (2010), 1987.

[21] D.H. Wang, D.W. Choi, J. Li, Z.G. Yang, Z.M. Nie, R. Kou, D.H. Hu, C.M. Wang, L.V. Saraf, J.G. Zhang, I.A. Aksay, J. Liu, Self-assembled TiO_2–graphene hybrid nanostructures for enhanced Li-ion insertion, ACS Nano 3, (2009), 907.

[22] C. Chen, W.M. Cai, M.C. Long, B.X. Zhou, Y.H. Wu, D.Y. Wu, Y.J. Feng, Synthesis of visible-light responsive graphene oxide/TiO_2 composites with p/n hetero-junction, *ACS Nano.* 4, (2010), 6425.

[23] H. Zhang, X.J. Lv, Y.M. Li, Y. Wang, J.H. Li, P25-graphene composite as a high performance photocatalyst, *ACS Nano.* 4, (2010), 380.

[24] Y.H. Zhang, Z.R. Tang, X.Z. Fu, Y.J. Xu, TiO_2–graphene nanocomposites for gas-phase photocatalytic degradation of volatile aromatic pollutant: Is TiO_2–Graphene truly different from other TiO_2–carbon composite materials, *ACS Nano*. 4, (2010), 7303.

[25] L.M. Peter, D.J. Riley, E.J. Tull, K.G.U. Wijayantha, Photosensitization of nanocrystalline TiO_2 by self-assembled layers of CdS quantum dots, Chem. Commun. *Cambridge.* 10, (2002), 1030.

[26] H. Su, Y. Xie, P. Gao, Y. Xiong, Y. Qian, Synthesis of MS/TiO_2 (M=Pb, Zn, Cd) nanocomposites through a mild sol–gel process, *J. Mater. Chem*. 11, (2001), 684.

[27] J.G. Lei, N. Qie, J. Zhou, Y.Y. Hua, T.H. Ji, Preparation and characterization of TiO_2 nanobelts deposited with Bi_2Se_3 nanoplates, *Mater. Letter.* 83, (2012), 108.

[28] T.T. ThanhThuy, H. Feng, Q.Y. Cai, Photocatalytic degradation of pentachlorophenol on ZnSe/TiO_2 supported by photo-Fenton system, *Chem. Eng. J.* 223, (2013), 379.

[29] L. Zhu, G. Trisha, C.Y. Park, Z.D. Meng, W.C. Oh, Enhanced Sonocatalytic Degradation of Rhodamine B by Graphene-TiO_2 Composites Synthesized by an Ultrasonic-Assisted Method, *Chinese. J. Catal.* 33, (2012), 1276.

[30] W.S. Hummers and R. E. Oûeman. Preparation of graphitic oxide, *J. Am. Chem. Soc.* 80, (1958), 1339.

[31] W.C. Oh, M.L. Chen, K. Zhang, F.J. Zhang, W. K. Jang, The effect of thermal and ultrasonic treatment on the formation of graphene-oxide nanosheets, *J. Korean Phys. Soc.* 56, (2010), 1097.

[32] T. N. Lambert, C. A. Chavez, B. Hernandez-Sanchez, P. Lu, N.S. Bell, A. Ambrosini, Synthesis and characterization of titania graphene nanocomposites, *J. Phys. Chem. C* 113, (2009), 19812.

[33] L. Zhu, S.B. Jo, S. Ye, K. Ullah and W.C. Oh, Sonophotocatalytic Performance of Bi_2Se_3-Graphene/TiO_2 Hybrid Nanomaterials Synthesized with a Microwave-assisted Method, *J. Korean Ceramic. Soc.* 51, (2014), 162.

[34] Y. Yu, W. T. Sun, Z. D. Hu, Q. Chen, L. M. Peng, Oriented Bi_2Se_3 nanoribbons film: structure, growth, and photoelectric properties, *Mater. Chem. Phys.* 124, (2010) 865.

[35] L. Zhu, S.B. Jo, S. Ye, K. Ullah and W.C. Oh, Rhodamine B degradation and reactive oxygen species generation by a ZnSe-graphene/TiO_2 sonocatalyst, *Chinese. J. Catal.* 35, (2014), 1825.

[36] M. Halajan, M.J. Torkamany, D. Dorranian, Effects of the ZnSe concentration on the structural and optical properties of ZnSe/PVA nanocomposite thin film, *J. Physics. Chem. Solids.* 75, (2014), 1187.